

# Performance and Complexity Analysis of Eigencombining, Statistical Beamforming, and Maximal-Ratio Combining

Constantin Siriteanu and Steven D. Blostein, *Senior Member, IEEE*

**Abstract**—For receive-side maximal-ratio combining (MRC) and maximum-average-SNR beamforming (BF), the wireless-channel fading correlation impacts the symbol-detection performance—decreasing correlation improves/degrades MRC/BF performance—whereas the numerical complexity of these methods is fixed—high/low for MRC/BF. Matching signal processing complexity to the actual correlation conditions and, thus, to the achievable performance is possible with a superset of MRC and BF known as maximal-ratio eigencombining (MREC). For imperfectly known and correlated fading gains, new closed-form expressions are derived for the probability density function of the MREC-output SNR, as well as for the outage probability (OP) and the average error probability. These new expressions permit seamless evaluation for any correlation value of MREC, MRC, and BF performance measures, such as the amount of fading, the deep-fade probability, diversity and array gains, and the OP. Our results confirm that, in realistic scenarios, adaptive MREC can achieve MRC-like performance for BF-like complexity.

**Index Terms**—Adaptive antenna arrays, array gain, channel estimation, diversity gain, eigencombining, Laplacian power azimuth spectrum (p.a.s.), lognormal azimuth spread (AS), numerical complexity, Rayleigh fading, statistical beamforming (BF).

## I. INTRODUCTION

SMART-ANTENNA-BASED wireless communications systems promise tremendous benefits in terms of data rate, user capacity, cell coverage, link quality, and transmitted signal energy [1]–[6]. For receive-side smart antennas, two conventional signal processing algorithms are as follows: 1) maximum average SNR beamforming (BF), which is also referred to as statistical BF [7], [8, Sec. 9.2.2], whereby the received signal vector is linearly combined with the dominant eigenvector of the correlation matrix of the channel gain vector; and 2) maximal-ratio combining (MRC) [6], [9], whereby the received signal vector is linearly combined with the channel gain vector.

BF and MRC are designed for particular spatial fading correlation conditions and only then yield significant performance

Manuscript received May 2, 2008; revised November 10, 2008. First published February 2, 2009; current version published August 14, 2009. This work was supported in part by The Korea Research Council of Fundamental Science and Technology and in part by The Natural Sciences and Engineering Research Council of Canada under Discovery Grant 4173. The review of this paper was coordinated by Prof. S. Cui.

C. Siriteanu is with the School of Computer Science and Engineering, Seoul National University, Seoul 151-742, Korea (e-mail: costi@cse.snu.ac.kr).

S. D. Blostein is with the Department of Electrical and Computer Engineering, Queen's University, Kingston, ON K7L 3N6, Canada (e-mail: steven.blostein@queensu.ca).

Digital Object Identifier 10.1109/TVT.2009.2014167

gains over the single-input–single-output (SISO) transceiver. The fading gains on the different received signal branches have to be fully correlated (coherent) for BF and uncorrelated for MRC [8, Sec. 9.2.2], [9]–[14]. However, actual signal arrival is characterized by a Laplacian power azimuth spectrum (p.a.s.) with small-to-moderate, lognormally distributed, and slowly varying azimuth spread (AS) [12, Sec. 4.2], [14]. The resulting variable antenna correlation yields unsteady BF and MRC performance, although the numerical complexity is fixed [13, Tab. II, p. 922]. Whereas BF may periodically underperform, MRC may have excessive numerical complexity, which leads to inefficient hardware usage [11].

Eigencombining, which is also known as eigenbeamforming [15], permits matching numerical complexity with actual channel correlation and, thus, with the achievable performance [11]–[14], [16], [17]. Maximal-ratio eigencombining (MREC) actually applies the principles of BF and MRC. First, the received signal vector is projected onto the dominant eigenvectors of the channel gain correlation matrix, i.e., the Karhunen–Loeve transform (KLT) [18]. Then, the resulting signals are processed according to the MRC criterion. The number of eigenvectors that are used in the KLT is referred to as the *MREC order* and determines the numerical complexity of the algorithm [12], [13].

Recently, several authors have analyzed, simulated, and implemented in digital devices receive-side eigencombining [10]–[13], [15], [19]. They compared the performance and the complexity of BF, MRC, and MREC for a perfectly known channel (p.k.c.) and for an imperfectly known channel (i.k.c.) whose fading gains are estimated by employing pilot-symbol-aided modulation (PSAM) at the transmitter and interpolation at the receiver [12, Secs. 2.5 and 3.6]. Importantly, BF and MRC were demonstrated to be performance-equivalent to the special cases of MREC, which helps simplify their analysis [12], [13].

Although this paper focuses on receive-side eigencombining, i.e., on single-input–multiple-output (SIMO) systems, transmit-side statistical eigenprocessing [i.e., for multiple-input–single-output (MISO) and multiple-input–multiple-output (MIMO)] has also recently been evaluated [14]. Finally, eigencombining has also been shown to benefit code-division multiple-access (CDMA) “rake” receivers that are affected by high intertap correlation [20].

As mentioned above, MREC can be viewed as a superset of MRC and BF. For MRC in a perfectly known Rayleigh fading channel, closed-form expressions for the probability density

function (pdf) and the cumulative distribution function (cdf) of the output SNR, as well as for the outage probability (OP), that appear in [3], [4], [6], [21], and [22] apply for correlated channel gains, but only when the eigenvalues of the channel correlation matrix are all distinct or all equal. However, in practice, channel fading is imperfectly known, and subsets of nearly equal eigenvalues can occur [12, Fig. 4.1], [13, Fig. 1].

For estimated fading but perfectly known related correlation matrices, optimum (*exact*) MRC is described in [12, App. A]. Given perfect knowledge of the channel *eigenstructure* (i.e., eigenvectors and eigenvalues), *exact MREC* is described in [13, Sec. III-D]. A simple, yet nonclosed-form, exact-MREC average error probability (AEP) expression that covers the case when some eigenvalues may be equal appears in [13, eq. (7), p. 919].

For i.k.c. and correlated fading, the suboptimum (*approximate*) implementation of MRC, which is described in [13, Sec. III-C1], has typically been analyzed with difficulty. The performance equivalence between this combining method and approximate MREC—which is described in [13, Sec. III-C1]—has produced a valuable, yet involved, closed-form AEP expression [13, eq. (37)] that allows for subsets of equal eigenvalues for the channel correlation matrix.

From here on, only *exact* (i.e., not *approximate*) MREC, BF, and MRC are considered. We derive new *closed-form expressions* for the pdf of the output SNR, as well as for the OP and the AEP, that apply seamlessly (for i.k.c. and for arbitrary relative eigenvalue magnitudes, i.e., any correlation between channel gains). These new expressions generalize those previously derived for MRC, BF, and MREC for ideal cases such as p.k.c. or uncorrelated spatial fading and for special cases such as those of all-equal or all-unequal correlation-matrix eigenvalues [3]–[6], [13], [14].

The newly derived expressions are then applied to study the exact-MREC performance, including BF and MRC as special cases, for i.k.c., and for continuous AS ranges (wherein some channel eigenvalues can become equal, which is a situation that cannot be handled with previous expressions [3]–[5]). We first look at qualitative performance indicators such as the amount of fading (AF) [6, eq. (2.5), p. 18] and *deep-fade probability* [23, p. 55]. Then, we evaluate quantitative indicators such as the *diversity gain* [1, Secs. 1.2.2 and 5.2] and the *array gain* [1, Secs. 1.2.1 and 5.3]. We find that low-order MREC can achieve near-MRC performance and, thus, can greatly outperform BF.

We already mentioned that the numerical complexity of BF and MRC is fixed, whereas their performance varies with the spatial correlation changes caused by fluctuating AS [13, Fig. 3]. The numerical complexities incurred by MREC, MRC, and BF—due to partial KLT (in BF and MREC), signal combining, and estimation of the time-varying channel gains and of the channel fading eigenstructure—were compared in [11]–[14], [16], and [17]. Adaptation of the MREC order, i.e., of the numerical complexity, to the correlation fluctuations in typical urban environments has previously been shown to yield near-MRC AEP performance, i.e., much better than BF, and lower average computational requirements [11], [13], [16], [17]. Using the new closed-form expressions derived

herein, we prove that exact MREC can also achieve near-MRC OP performance for significant computational savings.

The outline of this paper is as follows. Section II introduces the signal model, the combining methods (MREC, MRC, BF), and their relationships. Then, using a partial-fraction expansion of the reversed moment-generating function (r.m.g.f.) for the exact-MREC output SNR, we obtain closed-form expressions for the pdf and the cdf of this SNR and then for the OP and the AEP. Special cases of relative eigenvalue magnitudes (all equal, all distinct) are considered in the Appendix. In Section III, our newly derived performance-measure expressions are employed to comparatively evaluate the AF, the deep-fade probability, the array gain, and the diversity gain for MREC, MRC, and BF. Section IV compares the performance and the numerical complexity of MRC and BF versus MREC that is optimally adapted to the actual channel correlation for a typical urban scenario with a Laplacian p.a.s. and lognormal AS.

## II. SYMBOL-DETECTION PERFORMANCE MEASURES FOR EXACT MREC (MRC AND BF)

### A. Signal, Channel, and Noise Models

Although the principles of the ensuing analysis also apply for other multibranch receivers, including the CDMA “rake” [6], numerical examples are shown herein only for antenna arrays in frequency-flat fading.

Consider the signal model from [13, Sec. II], where the signal transmitted by a mobile station over a fading channel with Laplacian p.a.s. [14, eq. (15)] and lognormal AS [14, eq. (17)] is received at the base station with an  $L$ -element antenna array. The signal model is given by the  $L$ -dimensional vector equation

$$\tilde{\mathbf{y}} = \sqrt{E_s} b \tilde{\mathbf{h}} + \tilde{\mathbf{n}} \quad (1)$$

where  $E_s$  is the energy transmitted per symbol;  $b$  are the equiprobable unit-energy M-phase-shift-keying (M-PSK) symbols;  $\tilde{\mathbf{h}}$  is the channel fading gain vector, which is hereafter assumed zero-mean complex Gaussian (i.e., Rayleigh fading, unless stated otherwise) with correlation matrix  $\mathbf{R}_{\tilde{\mathbf{h}}}$ , i.e.,  $\tilde{\mathbf{h}} \sim \mathcal{N}_c(\mathbf{0}, \mathbf{R}_{\tilde{\mathbf{h}}})$ ; and  $\tilde{\mathbf{n}}$  is the zero-mean complex Gaussian spatially- and temporally-white noise with variance  $N_0$  per dimension, i.e.,  $\tilde{\mathbf{n}} \sim \mathcal{N}_c(\mathbf{0}, N_0 \mathbf{I})$ . We assume perfectly known the matrix  $\mathbf{U}$  containing the eigenvectors  $\mathbf{u}_i, i = 1, \dots, L \triangleq 1 : L$ , of  $\mathbf{R}_{\tilde{\mathbf{h}}}$ , and the diagonal matrix  $\mathbf{\Lambda}$  formed with corresponding eigenvalues  $\lambda_1 \geq \lambda_2 \geq \dots \geq \lambda_L$ . The components of  $\tilde{\mathbf{y}}$  are denoted hereafter as (signal) *branches*. The average per-branch per-symbol SNR is  $\Gamma_s \triangleq (E_s/N_0) \sigma_{h_i}^2$ , where  $\sigma_{h_i}^2$  is the variance of the  $i$ th component of the channel gain vector, which is assumed to be the same on all branches for our numerical results.

### B. MREC, MRC, and BF

MREC of order  $N \leq L$ , denoted hereafter with  $\text{MREC}_N$ , has been described in [13, Sec. III-A1] for p.k.c. as consisting of the following steps.

- 1) Perform the KLT of the  $L$ -dimensional received signal vector  $\tilde{\mathbf{y}}$  using the  $L \times N$  full-column-rank matrix  $\mathbf{U}_N$

formed with the first  $N$  eigenvectors of  $\mathbf{R}_{\tilde{\mathbf{h}}}$ . Mathematically, this can be written as  $\mathbf{y} = \sqrt{E_s} \mathbf{b} \mathbf{h} + \mathbf{n}$ , where  $\mathbf{y} = \mathbf{U}_N \tilde{\mathbf{y}}$ ,  $\mathbf{h} = \mathbf{U}_N \tilde{\mathbf{h}}$ , and  $\mathbf{n} = \mathbf{U}_N \tilde{\mathbf{n}}$ . The components of  $\mathbf{y}$  and  $\mathbf{h}$  are denoted as *eigenbranches* and *eigengains*, respectively. Since the columns of  $\mathbf{U}_N$  are orthonormal, for  $\mathbf{y}$ ,  $\mathbf{h}$ , and  $\mathbf{n}$ , the components are uncorrelated, and  $\mathbf{h} \sim \mathcal{N}_c(\mathbf{0}, \mathbf{\Lambda})$  and  $\mathbf{n} \sim \mathcal{N}_c(\mathbf{0}, N_0 \mathbf{I})$ .

- 2) Combine the  $N$ -dimensional vector  $\mathbf{y}$  with the eigengain vector  $\mathbf{h}$  according to the MRC criterion [9].

The practical case of i.k.c. occurs when the fading gains are estimated, e.g., through transmitter PSAM and receiver interpolation [12, Secs. 2.5.1, 2.5.2, and 3.6]. The numerical results shown herein employ the following estimation methods, which are detailed in [12, Sec. 3.6]: 1) SINC PSAM, which is a simple but suboptimum method, wherein the interpolator vector components are computed using a sinc function, and 2) MMSE PSAM, which is a complex but optimum method, wherein the interpolator is derived according to the MMSE criterion.

Given eigengain estimates and perfect knowledge of the channel eigenstructure, implementation of *optimal (exact) MREC* is described in [13, Sec. III-D]. A comparative analysis of the performance and the complexity of exact MREC, MRC, and BF is the goal of this paper. Therefore, let us now briefly review the relation of MREC with MRC and BF. MREC can be viewed as a superset of the traditional BF and MRC methods in that  $\text{MREC}_{N=1}$  represents statistical BF—an approach that is traditionally deployed at compact antennas in low-AS environments to take advantage of the array gain—whereas  $\text{MREC}_{N=L}$ , i.e., *full MREC*, is performance-equivalent with MRC of the original branches [13, Sec. III-D2]. MRC is traditionally deployed at widely spaced antennas to take advantage of diversity gain. Given channel gain estimates as well as knowledge of the channel correlation matrix and the cross-correlation matrix of the channel gain vector and its estimate, the optimal implementation of MRC, which is denoted hereafter as *exact MRC*, is detailed in [12, App. A].

### C. Symbol-Detection Performance Measures and Analysis Methods

Let us denote with  $\gamma$  the symbol-detection SNR at the output of a signal combiner, and let  $p(\gamma)$  denote the pdf of this SNR. The OP represents the probability that the probability of error  $P_e(\gamma)$  exceeds a threshold [6, Sec. 1.1.2, p. 5], i.e.,

$$P_o \triangleq \Pr [P_e(\gamma) > P_{e,\text{th}}]. \quad (2)$$

If the threshold SNR  $\gamma_{\text{th}}$  can be found so that  $P_{e,\text{th}} = P_e(\gamma_{\text{th}})$ , then the OP is also given by

$$P_o \triangleq \Pr(\gamma < \gamma_{\text{th}}) = \int_0^{\gamma_{\text{th}}} p(\gamma) d\gamma \quad (3)$$

which is the cdf of  $\gamma$  evaluated at  $\gamma_{\text{th}}$ .

For M-PSK transmission and maximum-likelihood symbol detection, the symbol error probability is given by [6, eq. (8.22), p. 198]

$$P_e(\gamma) = \frac{1}{\pi} \int_0^{\frac{M-1}{M}\pi} \exp\left(-\gamma \frac{g_{\text{PSK}}}{\sin^2 \phi}\right) d\phi, \quad g_{\text{PSK}} \triangleq \sin^2 \frac{\pi}{M}. \quad (4)$$

Then, the AEP [5, eq. (14.3–4), p. 817], [6, eq. (8.102), p. 219] is given by

$$\begin{aligned} P_e &\triangleq \int_0^\infty P_e(\gamma) p(\gamma) d\gamma \\ &= \frac{1}{\pi} \int_0^{\frac{M-1}{M}\pi} \int_0^\infty \exp\left(-\gamma \frac{g_{\text{PSK}}}{\sin^2 \phi}\right) p(\gamma) d\gamma d\phi \\ &= \frac{1}{\pi} \int_0^{\frac{M-1}{M}\pi} F_\gamma\left(\frac{g_{\text{PSK}}}{\sin^2 \phi}\right) d\phi \end{aligned} \quad (5)$$

where  $F_\gamma(s) \triangleq E\{e^{-s\gamma}\}$  is the *r.m.g.f.* of the SNR [6, eq. (1.2), p. 4]. The r.m.g.f. can readily be computed for various fading types [6, Tab. 2.2, p. 19]. The AEP derivation approach from (5) will be adopted in Section II-F.

### D. PDF of the Output SNR for Exact MREC

First, our assumptions of Gaussian noise and channel gains imply that the channel eigengains  $h_i \sim \mathcal{N}_c(0, \lambda_i)$  and their PSAM-based estimates  $g_i \sim \mathcal{N}_c(0, \sigma_{g_i}^2)$  are jointly Gaussian.

Then, the exact-MREC output SNR is given by [13, eq. (22)]

$$\gamma = \sum_{i=1}^N \gamma_i \quad (6)$$

where  $\gamma_i$  represents the SNR for the  $i$ th eigenbranch—i.e., the SNR obtained having knowledge of  $g_i$  and of the involved correlations—which is given by [13, eq. (19)]

$$\gamma_i \triangleq \frac{\frac{E_s}{N_0} \lambda_i |\mu_i|^2}{\frac{E_s}{N_0} \lambda_i (1 - |\mu_i|^2) + 1} \cdot \frac{|g_i|^2}{\sigma_{g_i}^2} \quad (7)$$

where  $\mu_i \triangleq \sigma_{h_i g_i} / \sqrt{\sigma_{h_i}^2 \sigma_{g_i}^2}$  is the correlation coefficient of  $h_i$  and  $g_i$ . The correlations that are required in (7) have been expressed for SINC and MMSE PSAM in [24, Tables 1 and 2]. Equation (6) indicates that the combiner maximizes the MREC SNR, which justifies the title of “exact MREC.”

Since  $g_i$  is Gaussian, the eigenbranch SNR  $\gamma_i$  from (7) has exponential pdf

$$p(\gamma_i) = \begin{cases} 1/\Gamma_i e^{-\gamma_i/\Gamma_i}, & \text{for } \gamma_i \geq 0 \\ 0, & \text{otherwise} \end{cases} \quad (8)$$

average

$$\Gamma_i \triangleq E\{\gamma_i\} = \frac{\frac{E_s}{N_0} \lambda_i |\mu_i|^2}{\frac{E_s}{N_0} \lambda_i (1 - |\mu_i|^2) + 1} \quad (9)$$

and variance [5, eqs. (2.1–113), p. 42]

$$\text{var}(\gamma_i) = E\{(\gamma_i - \Gamma_i)^2\} = \Gamma_i^2. \quad (10)$$

For p.k.c., we have  $\mu_i = 1$ , which reduces  $\gamma_i$  from (7) to  $\gamma_i = (E_s/N_0)|h_i|^2$  and its average to  $\Gamma_i = (E_s/N_0)\lambda_i$ .

For i.k.c., the r.m.g.f. of  $\gamma_i$  from (7) can readily be determined as [6, Tab. 2.2, p. 19]

$$F_i(s) \triangleq E\{e^{-s\gamma_i}\} = \int_0^\infty e^{-s\gamma_i} p(\gamma_i) d\gamma_i = \frac{1}{1 + s\Gamma_i}. \quad (11)$$

Then, using the independence of  $\gamma_i$ ,  $i = 1 : N$ , and (11), the r.m.g.f. of the output SNR  $\gamma$  from (6) can be written as

$$F_\gamma(s) = \prod_{i=1}^N \frac{1}{1 + s\Gamma_i}. \quad (12)$$

For certain AS values, some eigenvalues of  $\mathbf{R}_{\tilde{\mathbf{h}}}$  can become equal [13, Fig. 1]. Then, let  $\{\Xi_1, \Xi_2, \dots, \Xi_{N_d}\}$  denote the distinct values in the set  $\{\Gamma_1, \Gamma_2, \dots, \Gamma_N\}$ , so that

$$F_\gamma(s) = \prod_{k=1}^{N_d} \frac{1}{(1 + s\Xi_k)^{r_k}} \quad (13)$$

where  $r_k$  denotes the algebraic multiplicity of  $\Xi_k$ ,  $k = 1 : N_d$ , with  $\sum_{k=1}^{N_d} r_k = N$ . Applying to (13) the partial fraction expansion from [25, Sec. 2.102, pp. 56–57] yields

$$F_\gamma(s) = \frac{1}{A} \sum_{k=1}^{N_d} \sum_{l=1}^{r_k} c_{k,l} \frac{1}{(s + 1/\Xi_k)^l} \quad (14)$$

where  $A \triangleq \prod_{k=1}^{N_d} \Xi_k^{r_k} = \prod_{i=1}^N \Gamma_i$ , and the factor  $c_{k,l}$  is given by

$$c_{k,l} \triangleq \frac{A}{(r_k - l)!} \left\{ D_s^{(r_k - l)} \left[ F_\gamma(s) \cdot \left( s + \frac{1}{\Xi_k} \right)^{r_k} \right] \right\} \Big|_{s = -1/\Xi_k}$$

with  $D_s^{(n)}[G(s)] \triangleq d^n[G(s)]/ds^n$ , i.e., the  $n$ th derivative of  $G(s)$ . Then,  $c_{k,l}$  can be expressed in closed form as [12, eq. (3.166), p. 114]

$$c_{k,l} = (-1)^{r_k - l} \cdot \sum_{\Omega_i} \prod_{\substack{j=1 \\ j \neq k}}^{N_d} d_j \cdot \left( \frac{1}{\Xi_j} - \frac{1}{\Xi_k} \right)^{-(r_j + i_j)} \quad (15)$$

for  $k = 1 : N_d$  and  $l = 1 : r_k$ , where  $\Omega_i$  stands for the set of integers  $\{i_j, j = 1 : N_d, j \neq k \mid 0 \leq i_j \leq r_k - l, \sum_{j=1, j \neq k}^{N_d} i_j = r_k - l\}$ , and  $d_j = \binom{r_j - 1 + i_j}{i_j}$  is the binomial coefficient.

Now, using the Laplace-transform pair

$$\frac{1}{(s + 1/\Xi_k)^l} \xleftrightarrow{\mathcal{L}} \frac{\gamma^{l-1} e^{-\gamma/\Xi_k}}{(l-1)!} \quad (16)$$

the inverse Laplace transform of (14) yields the following novel closed-form expression for the pdf of  $\gamma$  for exact MREC in the most general case when some eigenvalues can coincide:

$$p(\gamma) = \frac{1}{A} \sum_{k=1}^{N_d} \sum_{l=1}^{r_k} c_{k,l} \cdot \frac{\gamma^{l-1} e^{-\gamma/\Xi_k}}{(l-1)!}. \quad (17)$$

The Appendix specializes the above derivations for the channel correlation matrix with all-equal or all-distinct eigenvalues, matching previously derived pdf expressions.

Since  $\text{MREC}_{N=1}$  represents BF and since  $\text{MREC}_{N=L}$  (full MREC) is performance-equivalent with MRC, (17) also describes BF and MRC performance. Our MREC-based approach greatly simplifies MRC performance analysis for correlated and imperfectly-known channel gains.

### E. Exact-MREC Output SNR CDF and OP

The cdf of  $\gamma$  can now be obtained from (17) as

$$P(\gamma) = \frac{1}{A} \sum_{k=1}^{N_d} \sum_{l=1}^{r_k} c_{k,l} \Xi_k^l \left[ 1 - e^{-\gamma/\Xi_k} \sum_{n=1}^l \frac{(\gamma/\Xi_k)^{n-1}}{(n-1)!} \right]. \quad (18)$$

Since the cdf implicitly depends on  $\Gamma_s$ , we will also write it as  $P(\gamma; \Gamma_s)$ . Using this cdf expression, the OP, which is defined in (2), can be written in closed form for exact MREC (MRC and BF) as follows:

$$P_o = P(\gamma = \gamma_{\text{th}}; \Gamma_s). \quad (19)$$

The Appendix specializes (18) and (19) to the cases of all-equal and all-distinct eigenvalues, matching previously derived expressions.

### F. Exact-MREC AEP

Substituting (12) in the r.m.g.f.-based AEP derivation procedure described in Section II-C yields the following expression for the AEP of exact MREC [13, eq. (28)]:

$$\begin{aligned} P_{e,N} &= \frac{1}{\pi} \int_0^{\frac{M-1}{M}\pi} F_\gamma \left( \frac{g_{\text{PSK}}}{\sin^2 \phi} \right) d\phi \\ &= \frac{1}{\pi} \int_0^{\frac{M-1}{M}\pi} \prod_{i=1}^N \left( 1 + \Gamma_i \frac{g_{\text{PSK}}}{\sin^2 \phi} \right)^{-1} d\phi. \end{aligned} \quad (20)$$

Although a nonclosed form, this finite-limit-integral AEP expression can readily be computed. Note that (20) extends to i.k.c. the results that are obtained for p.k.c. in [6, Sec. 9.2.3] and [14, eq. (82)].

A closed-form MREC AEP expression can also be derived as follows. Using the first equality in (20) along with (14), the exact-MREC AEP expression for the most general case when

some eigenvalues may be equal can be recast in the following canonical form:

$$P_{e,N} = \frac{1}{A} \sum_{k=1}^{N_d} \sum_{l=1}^{r_k} c_{k,l} \cdot \Xi_k^l \cdot I_l(\Xi_k) \quad (21)$$

where

$$I_l(\Xi_k) \triangleq \frac{1}{\pi} \int_0^{\frac{M-1}{M}\pi} \left[ 1 + \Xi_k \frac{g_{\text{PSK}}}{\sin^2 \phi} \right]^{-l} d\phi \quad (22)$$

is expressed in closed form in the Appendix [see (33)]. Note that (21) is not as straightforward to compute as (20) is because factors  $c_{k,l}$  from (15) depend on the relative magnitudes of the eigenvalues of  $\mathbf{R}_{\tilde{\mathbf{h}}}$ . The Appendix also specializes the above AEP expressions to the cases of all-equal and all-distinct eigenvalues, matching previous results.

### G. Extensions to Other Modulation, System, and Fading Cases

As indicated in [6, Ch. 8] and [26, Ch. 4], the bit or symbol error probabilities, or the tight bounds on them, can be written similarly to (4) for modulations other than M-PSK (e.g., M-quadratic-amplitude modulation—M-QAM). Furthermore, the symbol-detection SNR for optimum combining can be written as a sum of possibly correlated exponentially distributed branch SNRs also for MISO and MIMO systems, e.g., for transmit MRC [1, eq. (5.30), p. 96] and space-time block coding [1, eq. (5.38), p. 97]. Such a combiner-output-SNR expression can be recast as a sum of uncorrelated exponentially distributed random variables with averages that are given by the eigenvalues of the channel gain vector correlation matrix [26, eq. (4.4.6), p. 53]. Then, performance measures (the SNR pdf, the OP, and the AEP) for these modulations and systems can be derived as above.

Finally, for Ricean fading [6, Ch. 2], the approaches described above apply after replacing correlations with autocorrelations and cross correlations with cross covariances. Furthermore, the pdf and the r.m.g.f. of the eigenbranch SNR  $\gamma_i$  can then be derived from [6, Tab. 2.2, p. 19]. Therefore, an AEP expression that is similar to (20) is readily obtainable. However, the r.m.g.f. of the MREC output SNR can be written in a product form whose terms contain a fraction, similarly to (12), but also an exponential factor. Consequently, it is not known how this r.m.g.f. could be recast as a sum of its component terms, as in (14), and closed-form expressions for the performance measures discussed above could not be obtained.

## III. PERFORMANCE EVALUATION FOR EXACT MREC VERSUS MRC AND BF

### A. Settings for Numerical Experiments

The following performance evaluation for MREC, BF (i.e.,  $\text{MREC}_{N=1}$ ), MRC (i.e.,  $\text{MREC}_{N=L}$ ), and SISO (i.e.,  $\text{MREC}_{L=N=1}$ ) employs the expressions derived in Section II for the pdf and the cdf of the output SNR, as well as for the OP

and the AEP. Consider a receiving uniform linear array (ULA) with  $L = 5$  and normalized interelement distance  $d_n = 1$  (i.e., the actual distance is equal to half of the carrier wavelength) and an intended signal arriving with a Laplacian p.a.s. [14], with a mean angle of arrival  $\theta_c = 0$  (i.e., the direction perpendicular on the antenna array). The channel gains have equal variance. The maximum normalized Doppler shift (Doppler shift divided by the symbol frequency) is set to 0.01 [12, eq. (2.48), p. 21], [13, Tab. I]. Channel estimation relies on SINC or MMSE PSAM with slot length  $M_s = 7$  (six data symbols and one pilot symbol) and interpolator length  $T = 11$  (the pilot samples from 11 surrounding slots are interpolated to yield the required estimate) [12, Sec. 3.6, p. 81].

### B. Evaluation of the PDF of the Output SNR

An  $L$ -element antenna array collects  $L$  times more intended-signal energy than each of its constituent elements on average over the fading. Suitable combining of the received signals can transform this additional received intended-signal energy into an array gain, as discussed in Section III-E. For now, only the effects of channel gain correlation and the combiner type on the pdf of the combiner output SNR are of interest. Thus, the numerical results discussed here have been obtained under the condition that the average output SNRs for a SIMO ULA and a SISO receive antenna are equal. This is equivalent to assuming that, when an  $L$ -element ULA is employed,  $L$  times less energy is transmitted than in the SISO case.

Fig. 1 shows several pdf-related plots that were computed using (17) for p.k.c. versus the output SNR  $\gamma$  and the AS [13]. The surface represents the pdf of the output SNR of  $\text{MREC}_{N=3}$ , which is denoted hereafter as  $p_{\text{MREC},N=3}(\gamma; \text{AS})$ . Also shown are the peaks of the SNR pdf surfaces corresponding to SISO, BF, MRC, and  $\text{MREC}_{N=2:4}$  because they reveal the shapes of the corresponding surfaces, circumventing the need to separately plot each of them. Furthermore, the peak of the pdf indicates the most likely SNR value, providing insight into the performance.

Fig. 1 indicates that:

- For AS = 0, all combiners yield the same output-SNR pdf, which decreases when  $\gamma$  increases. The explanation follows. For AS = 0, the channel gains are coherent, and therefore,  $\Gamma_1 \neq 0$  and  $\Gamma_{2:L} = 0$ —see [12, Prop. 1, p. 54], [14, Prop. 1]. Then,  $\text{MREC}_{N=2:L}$  reduces to BF, whose output SNR is distributed exponentially—see (8). The SISO and BF SNR pdf's also coincide at AS = 0 because we assumed an equal average output SNR for SISO and the SIMO ULA.
- The pdf of the SISO output SNR is AS-independent, as expected.
- $p_{\text{SISO,BF}}(\gamma \uparrow; \forall \text{AS}) \downarrow$ , i.e., when  $\gamma$  increases, the output-SNR pdf decreases, at any AS value, which means that for SISO and BF, the SNR pdf is a decreasing function of  $\gamma$ .
- $\max_{\gamma} [p_{\text{BF}}(\gamma, \text{AS} \uparrow)] \uparrow$ , i.e., BF yields higher probabilities of low SNR values (worse performance) with increasing AS due to an increasing mismatch between the BF weights—the components of the dominant eigenvector of  $\mathbf{R}_{\tilde{\mathbf{h}}}$  (see [13, eq. (5), for  $N = 1$ ] and [14, eq. (32)])—and

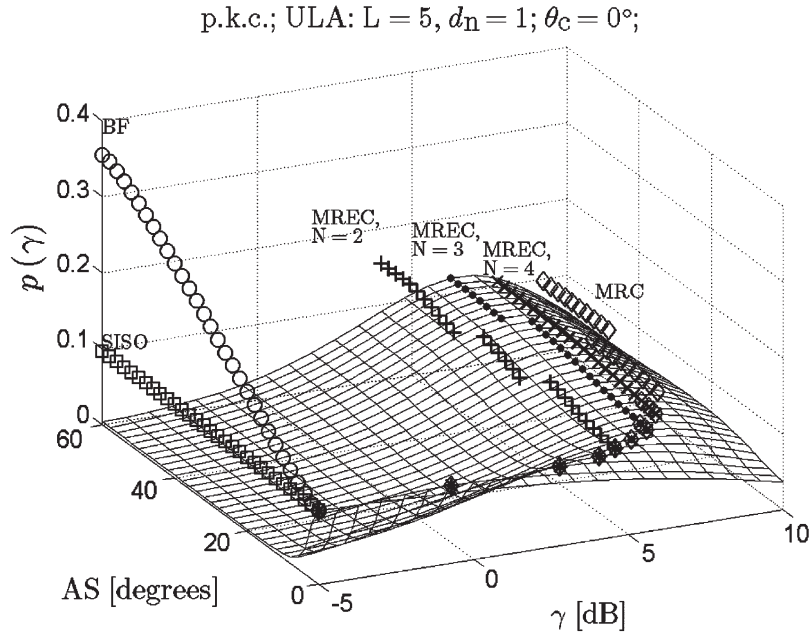


Fig. 1. Output-SNR pdf for p.k.c. and equal average SNR for SISO and SIMO ULA employing BF, MRC, and MREC.

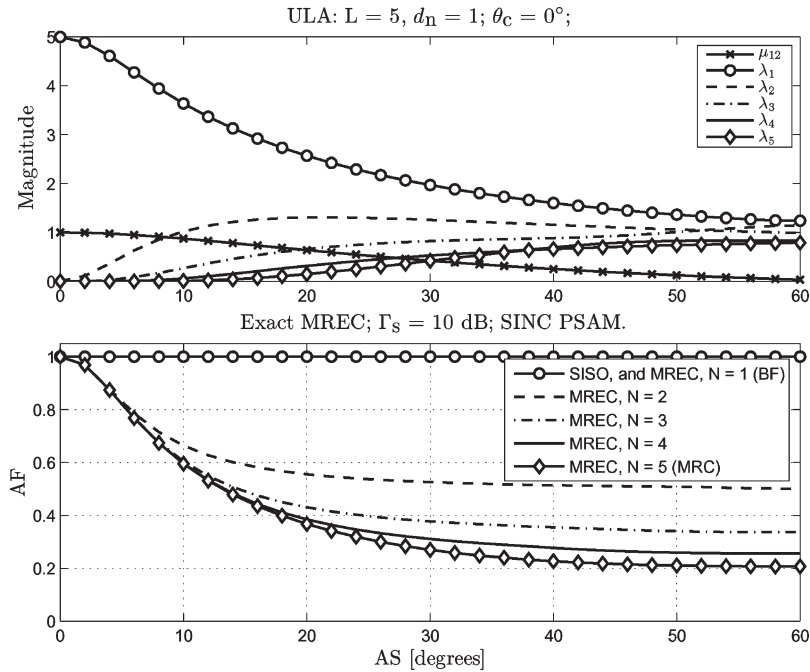


Fig. 2. (Top) Correlation coefficient of fading at adjacent array elements,  $\mu_{1,2} = (\mathbf{R}_{\mathbf{h}})_{12}$ , and eigenvalues of  $\mathbf{R}_{\mathbf{h}}$ ,  $\lambda_i, i = 1 : L$ . (Bottom) AF for SISO and exact MREC (including BF and MRC) for SINC PSAM.

the corresponding channel gains. This diminishes the array gain, as discussed in Section III-E.

- For  $AS \neq 0$ , the SNR pdf plots for  $MREC_{N \geq 2}$  have different shapes than for SISO and BF, which is due to different distribution types—compare (8) and (17).
- Since  $MREC_{N=3}$  collects the intended-signal and noise energy along the first  $N = 3$  channel eigenvectors,  $\arg \max_{\gamma} [p_{MREC_{N=3}}(\gamma; AS \uparrow_0^{44^\circ})] \uparrow$  and  $\arg \max_{\gamma} [p_{MREC_{N=3}}(\gamma; AS \uparrow_{12}^{44^\circ})] \approx 7$  dB. At very low AS, the intended-signal energy is concentrated along a single eigenvector, as shown in the top subplot in Fig. 2

(see also [13, Fig. 1] and [14, Fig. 1]). For increasing AS, the intended-signal energy is distributed more uniformly over the channel eigenvectors. Combining the corresponding (uncorrelated) channel eigengains increases the likelihood of higher SNR values. On the other hand,  $\arg \max_{\gamma} [p_{MREC_{N=3}}(\gamma; AS \uparrow_{46}^{60^\circ})] \approx 6.25$  dB, i.e., lower than  $\arg \max_{\gamma} [p_{MREC_{N=3}}(\gamma; AS \uparrow_{12}^{44^\circ})] \approx 7$  dB, because for  $AS \in [46^\circ, 60^\circ]$ , eigenvalues  $\lambda_1, \lambda_2$ , and  $\lambda_3$  convey less than 70% of the total average intended-signal energy, as shown in the top subplot in Fig. 2, as well as in [13, Fig. 1] and [14, Fig. 1]. The remainder is lost due

to the mismatch between combiner weights and channel gains. This high-AS degrading effect is more pronounced for smaller  $N$ .

- Confirming that MRC inherently takes advantage of the intended-signal energy arriving over all  $L$  eigen-vectors, we find that  $\arg \max_{\gamma} [p_{\text{MRC}}(\gamma, \text{AS} \uparrow_{0^{\circ}}^{60^{\circ}})] \uparrow$  and  $\arg \max_{\gamma} [p_{\text{MRC}}(\gamma, \text{AS} \uparrow_{42^{\circ}}^{60^{\circ}})] \approx 9.25$  dB.
- Interestingly, for AS below a certain value, which increases with increasing  $N$ ,  $p_{\text{MREC},N}(\gamma; \text{AS}) \approx p_{\text{MRC}}(\gamma; \text{AS})$ , i.e.,  $\text{MREC}_N$  can yield MRC-like performance.

For i.k.c., we obtained similar pdf plots as above for p.k.c. However, MMSE PSAM yields

- $\arg \max_{\gamma} [p_{\text{MREC}_{N=3}}(\gamma, \text{AS} \uparrow_{0^{\circ}}^{28^{\circ}})] \uparrow$
- $\arg \max_{\gamma} [p_{\text{MREC}_{N=3}}(\gamma, \text{AS} \uparrow_{18^{\circ}}^{28^{\circ}})] \approx 6.25$  dB
- $\arg \max_{\gamma} [p_{\text{MREC}_{N=3}}(\gamma, \text{AS} \uparrow_{30^{\circ}}^{60^{\circ}})] \approx 5.5$  dB

implying some performance degradation compared to p.k.c. On the other hand, the simple SINC PSAM method yields a much more significant performance deterioration, as follows:

- $\arg \max_{\gamma} [p_{\text{MREC}_{N=3}}(\gamma, \text{AS} \uparrow_{0^{\circ}}^{44^{\circ}})] \uparrow$
- $\arg \max_{\gamma} [p_{\text{MREC}_{N=3}}(\gamma, \text{AS} \uparrow_{14^{\circ}}^{44^{\circ}})] \approx 3.25$  dB
- $\arg \max_{\gamma} [p_{\text{MREC}_{N=3}}(\gamma, \text{AS} \uparrow_{46^{\circ}}^{60^{\circ}})] \approx 2.5$  dB.

Comparing these results with those described above for p.k.c. indicates that channel estimation results in additional combiner-channel mismatch loss for  $\text{MREC}_{N < L}$ . Estimation errors also deteriorate MRC performance:  $\arg \max_{\gamma} [p_{\text{MRC},\text{p.k.c.}}(\gamma, \text{AS} = 60^{\circ})] \approx 9.25$  dB, whereas  $\arg \max_{\gamma} [p_{\text{MRC},\text{MMSE}}(\gamma, \text{AS} = 60^{\circ})] \approx 7.75$  dB and  $\arg \max_{\gamma} [p_{\text{MRC},\text{SINC}}(\gamma, \text{AS} = 60^{\circ})] \approx 5.5$  dB.

### C. Amount of Fading

Given the distribution of the output SNR of a combiner  $\gamma$ , one can measure fading severity by the AF, which is defined as [6, eq. (2.5), p. 18]

$$\text{AF}(\gamma) \triangleq \frac{\text{var}(\gamma)}{(E\{\gamma\})^2} = \frac{E\{\gamma^2\} - (E\{\gamma\})^2}{(E\{\gamma\})^2}. \quad (23)$$

The AF describes the variability of the SNR relative to its average and is typically independent of  $E\{\gamma\}$  [6, p. 18]. The Rayleigh fading SISO case yields  $\text{AF} = 1$  and, thus, provides a convenient reference. Smaller AF indicates less severe fading experienced at the combiner output, i.e., better performance.

For Rayleigh fading and exact MREC, the individual eigen-branch SNRs, i.e.,  $\gamma_i, i = 1 : L$ , defined in (7) are mutually uncorrelated and exponentially distributed random variables, with averages and variances expressed in (9) and (10), respectively. The exact-MREC output SNR defined in (6) is given by the sum of these individual SNRs. Then, it can be shown that the AF for order- $N$  exact MREC satisfies the following inequalities:

$$\frac{1}{N} \leq \text{AF}(\gamma; N) = \frac{\sum_{i=1}^N \Gamma_i^2}{\left(\sum_{i=1}^N \Gamma_i\right)^2} \leq 1. \quad (24)$$

ULA:  $L = 5, d_n = 1, \theta_c = 0$ ; Exact MREC,  $N = 3$ ; SINC PSAM.

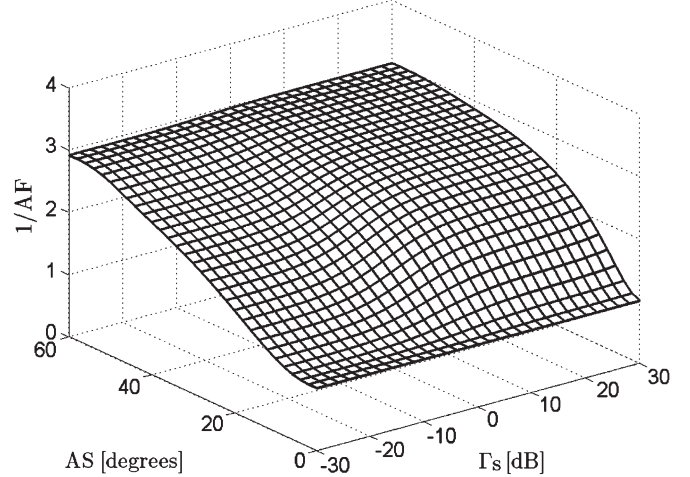


Fig. 3. Inverse of the AF ( $1/\text{AF}$ ) for exact  $\text{MREC}_{N=3}$  with SINC PSAM.

Based on [27, Sec. 3.2.9, p. 11], the lower bound is achieved for identically distributed eigenbranches, i.e., when  $\Gamma_1 = \Gamma_2 = \dots = \Gamma_N$ . For  $N = L$ , this implies independent identically distributed channel gains based on [12, Prop. 2, p. 54] and [14, Prop. 2]. The upper bound in (24) is achieved when  $\Gamma_1 \neq 0$  and  $\Gamma_2 = \dots = \Gamma_L = 0$ , which implies coherent branches, based on [12, Prop. 1, p. 54] and [14, Prop. 1].

Fig. 2 displays versus the AS the following:

- 1) In the top subplot, the correlation coefficient of the channel gains at adjacent antenna elements  $\mu_{12}$  and the eigenvalues of  $\mathbf{R}_h$ , i.e.,  $\lambda_i, i = 1 : L$ ;
- 2) In the bottom subplot, the AF for SISO and an ULA with exact MREC (including BF and MRC) for SINC PSAM.

Note first that due to the continuous changes in the relative magnitudes of the eigenvalues, this figure could not have been obtained using previously available SNR pdf expressions [3], [4]. Then, note that, as SISO, BF yields  $\text{AF} = 1$ , i.e., no fading reduction. On the other hand, the fading-reduction capabilities of  $\text{MREC}_{N=2}$  equal those of MRC for  $\text{AS} \leq 6^{\circ}$  and improve further before reaching a floor for  $\text{AS} \approx 25^{\circ}$ . This floor is inversely proportional to the MREC order, which is in agreement with the lower bound in (24). The intuitive explanation is that, for large AS, MREC combines  $N$  uncorrelated channel eigengains of similar strengths, thus reducing fading  $N$ -fold (see also Section A of the Appendix).

Fig. 3 shows  $1/\text{AF}$  that is computed using (24) for exact  $\text{MREC}_{N=3}$  with SINC PSAM. Similar (not shown) results have been obtained for MMSE PSAM. Very small AS yields  $\text{AF} \approx 1, \forall N$ , reflecting a lack of diversity, whereas AS  $\uparrow$  yields  $[\text{AF}^{-1}] \uparrow_1^N$  at any value of  $\Gamma_s$ .

### D. Evaluation of the SNR CDF, the Deep-Fade Probability, and the OP

Fig. 4 plots the output-SNR cdf computed using (18) for exact  $\text{MREC}_{N=3}$ , SINC PSAM, unit-variance channel gains (assumed hereafter for ULA and SISO), and  $\Gamma_s = E_s/N_0 = 10$  dB. The slope of  $P(\gamma; \text{AS} = 0)$  is unitary [also for all other MREC orders, as other results have indicated (not shown

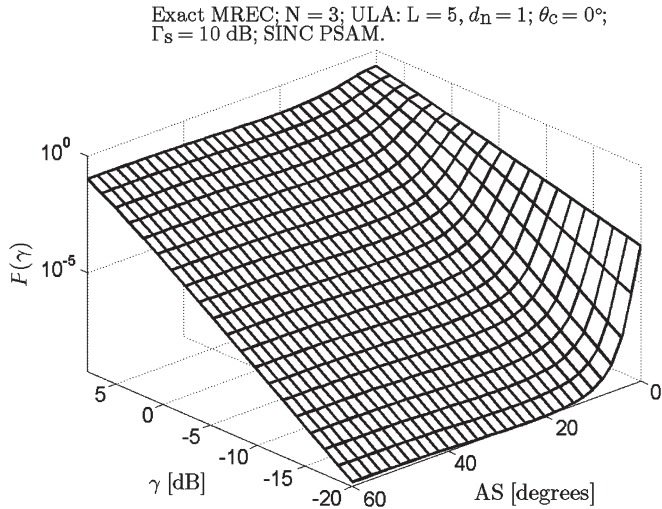


Fig. 4. The cdf of the instantaneous output SNR for exact MREC<sub>N=3</sub>, with SINC PSAM and  $\Gamma_s = 10$  dB.

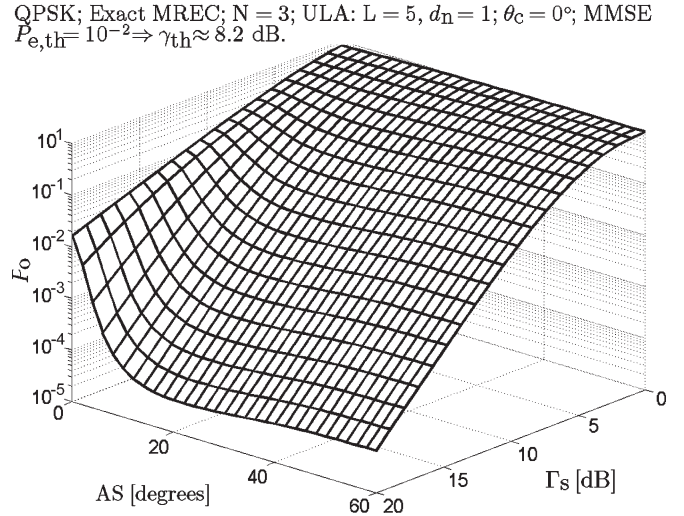


Fig. 5. OP for exact MREC<sub>N=3</sub>, MMSE PSAM, QPSK, and  $P_{e,th} = 10^{-2}$ , i.e.,  $\gamma_{th} \approx 8.2$  dB.

TABLE I  
DEEP-FADE PROBABILITY,  $\Pr(\gamma \leq 0 \text{ dB}; \Gamma_s = 30 \text{ dB})$

Combiner	Channel info	AS = 0°	AS = 10°	AS = 20°
BF	p.k.c.	$10^{-3.70}$	$10^{-3.56}$	$10^{-3.41}$
	MMSE	$10^{-3.58}$	$10^{-3.44}$	$10^{-3.29}$
	SINC	$10^{-3.33}$	$10^{-3.21}$	$10^{-3.08}$
MREC <sub>N=3</sub>	p.k.c.	$10^{-3.79}$	$10^{-9.78}$	$10^{-10.12}$
	MMSE	$10^{-3.61}$	$10^{-9.45}$	$10^{-9.79}$
	SINC	$10^{-3.34}$	$10^{-8.83}$	$10^{-9.18}$
MRC	p.k.c.	$10^{-3.79}$	$10^{-13.85}$	$10^{-16.08}$
	MMSE	$10^{-3.61}$	$10^{-13.33}$	$10^{-15.56}$
	SINC	$10^{-3.32}$	$10^{-12.31}$	$10^{-14.57}$

here)]. On the other hand, the slope of  $P(\gamma; AS \uparrow_{0^\circ}^{20^\circ})$  increases. For large AS, this slope becomes proportional to the MREC order  $N$ .

The cdf of the combiner output SNR can be used to evaluate receiver performance in fading channels through the *deep-fade probability* [23, p. 55]. A deep fade is defined as the situation in which, although  $\Gamma_s$  is large, the output SNR is subunitary (i.e., below 0 dB). Table I shows this probability for exact BF, MREC<sub>N=3</sub>, and MRC for  $\Gamma_s = 30$  dB and AS = 0, 10°, and 20°. For AS = 0, BF, MREC, and MRC coincide. With increasing AS, the BF performance degrades, whereas MREC and MRC yield significant improvements. MREC can actually yield a significant proportion of the MRC performance.

Fig. 5 displays the exact-MREC<sub>N=3</sub> OP computed using (19) for MMSE PSAM, and QPSK threshold error probability  $P_{e,th} = 10^{-2}$ , which, based on (4), corresponds to  $\gamma_{th} \approx 8.2$  dB. At high  $\Gamma_s$ , the magnitude of the slope of  $P_o(\Gamma_s)$  is 1 for AS = 0 and increases with increasing AS, reaching a maximum of 3 for AS  $\approx 20^\circ$ . This and other (not shown) results reveal that, at high AS, the high- $\Gamma_s$  OP slope magnitude is given by the MREC order. Furthermore, the minimum AS that maximizes the slope magnitude increases with an increasing MREC order. The high- $\Gamma_s$  slope of symbol-detection performance measures reveals the benefits of diversity combining in fading channels and is known as the *diversity order* [26].

QPSK; ULA: L = 5,  $d_n = 1$ ,  $\theta_c = 0^\circ$ ; Exact MREC, N = 3; MMSE PSAM.

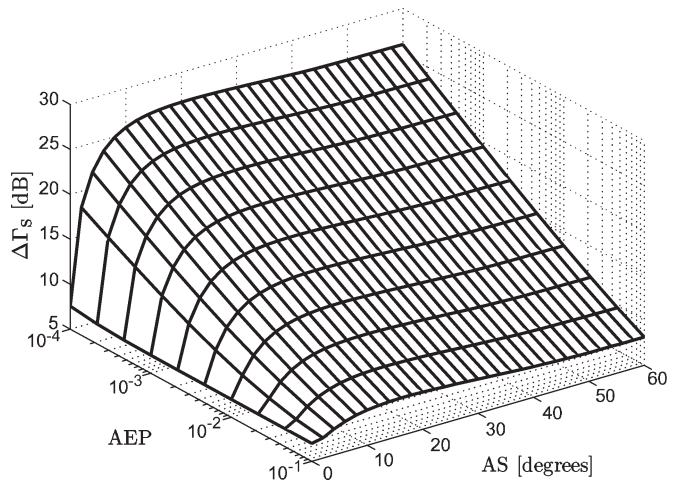


Fig. 6. Reduction in the average SNR that is required to attain a given AEP with MREC<sub>N=3</sub> instead of SISO, for QPSK and MMSE PSAM.

E. Array Gain, Mismatch Loss, and Diversity Gain

The AF, the deep-fade probability, and the diversity order are qualitative indicators of the fading-reduction capabilities of combiners. It would be more practical to determine, as shown next, how much energy the mobile station can save when the base station receiver employs a multibranch combiner compared with the SISO case. Toward this end, the AEP expression from (20) is numerically inverted to determine the  $\Gamma_s$  values that are necessary for MREC and SISO to achieve a given AEP. Their difference

$$\Delta\Gamma_s = \Gamma_{s,SISO} - \Gamma_{s,MREC} \text{ [dB]} \tag{25}$$

is the SNR gain of MREC over SISO.

Fig. 6 shows this gain versus AEP and AS for exact MREC<sub>N=3</sub> for QPSK and MMSE PSAM. For AS = 0, the AEP level does not affect  $\Delta\Gamma_s$ . This is because only one channel eigenvalue is then nonzero [12, Prop. 1, p. 54],

[14, Prop. 1], and, thus, the corresponding eigenvector conveys all the intended-signal energy. Therefore,  $\text{MREC}_{vN}$  reduces to BF in this case. The output-SNR distribution is then an exponential one for MREC and SISO. Thus, for  $\text{AS} = 0$ , MREC can only provide an average-output-SNR gain over SISO. Such an increase is commonly known as *array gain* [1, Secs. 1.2.2 and 5.2].

Let us investigate further the MREC array gain. Using (6), the average output SNR for exact  $\text{MREC}_N$  can be written as

$$\Gamma \triangleq E\{\gamma\} = \sum_{i=1}^N \Gamma_i \quad (26)$$

where  $\Gamma_i > 0$ ,  $i = 1 : N$ , are the eigenbranch average SNRs defined in (9). Then, the array gain is the ratio of the MREC and SISO average output SNRs, i.e.,

$$\text{AG} = \frac{\Gamma}{\Gamma_0} \quad (27)$$

which, for identically distributed and perfectly-known channel gains, can be written as

$$\text{AG} = 10 \log_{10} \left( L \frac{\sum_{i=1}^N \lambda_i}{\sum_{i=1}^L \lambda_i} \right) \in [10 \log_{10} N, 10 \log_{10} L]. \quad (28)$$

The upper bound is achieved for coherent channel gains; that is, for  $\text{AS} = 0$ , the MREC array gain is proportional to the number of branches  $L$ . Fig. 6 actually reveals that  $\Delta\Gamma_s \approx 7 \approx 10 \log_{10} L|_{L=5}$  dB at  $\text{AS} = 0$ .

The MREC array gain lower bound from (28), i.e.,  $10 \log_{10} N$ , is achieved for uncorrelated channel gains. Low correlation is incurred for large AS, as shown in the top subplot in Fig. 2. Thus, when AS increases from zero to large values, the array gain diminishes from  $10 \log_{10} L$  to  $10 \log_{10} N$ .

Let us first consider the case of BF, i.e.,  $\text{MREC}_{N=1}$ . Then, the array gain decreases from  $10 \log_{10} L$  to 0. This is verified in Fig. 7, which displays contours that are obtained by slicing at  $\text{AEP} = 10^{-3}$  surfaces as that shown in Fig. 6 for all  $N = 1 : L$ . Recall that BF does not offer fading reduction over SISO. Thus, the  $\Delta\Gamma_s$  plot shown in Fig. 7 for BF actually represents the array gain only. For  $\text{AS} = 0$ , the BF weight vector (the dominant eigenvector) is perfectly aligned with the channel gain vector, and, thus, BF maximizes the array gain. With increasing AS, there is an increasing mismatch between the BF weights and the channel gains. The mismatch loss will diminish and ultimately cancel the BF array gain.

As Fig. 7 indicates,  $\text{MREC}_{1 < N < L}$  can also incur noticeable mismatch loss. After  $\Delta\Gamma_s$  peaks at an AS value that is proportional to  $N$ ,  $\Delta\Gamma_s$  suffers a reduction that is inversely proportional to  $N$ . The explanation for the mismatch loss in  $\text{MREC}_{1 < N < L}$  is a simple generalization of the explanation given above for BF. Assuming p.k.c., the  $\text{MREC}_{N < L}$  weight vector with respect to the received signal vector  $\tilde{\mathbf{y}}$  can be shown to be  $\mathbf{U}_N \mathbf{U}_N^H \tilde{\mathbf{h}}$ , i.e., nonidentical to the channel vector  $\tilde{\mathbf{h}}$ , which would be required for perfect combining. Nonetheless, given  $N$ , these two vectors nearly coincide for AS below the value for which most of the intended-signal energy arrives

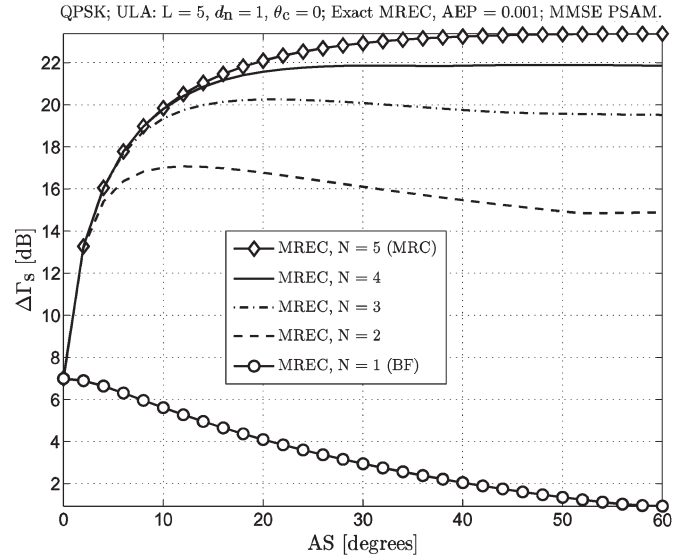


Fig. 7. SNR gain achieved with exact  $\text{MREC}_{N=1:5}$  over SISO for QPSK, MMSE PSAM, and  $\text{AEP} = 10^{-3}$ .

along the  $N$  selected eigenvectors. For higher AS, the intended-signal energy arrives from directions that are unaccounted for by the weight vector deployed by  $\text{MREC}_N$ , yielding higher mismatch loss. Higher  $N$  ensures that this mismatch loss begins affecting the performance at higher AS and that the loss is smaller. Clearly, there is no such mismatch loss for full MREC (MRC) because the receiver weight vector matches the channel vector. This is confirmed by the line corresponding to MRC in Fig. 7.

Figs. 6 and 7 show that  $\Delta\Gamma_s$  initially increases with AS increasing from zero, which represents the *diversity gain* [1, Secs. 1.2.2 and 5.2]. Increasing AS yields decreasing channel gain correlation, and thus, the peaks of the SNR pdf occur at larger SNR values (see Fig. 1). This reduces the AF and the deep-fade probability and increases the magnitude of the slope of  $\text{AEP}(\Gamma_s)$ , i.e., the diversity order. In Fig. 6, the SNR gain is larger for a smaller AEP because the AEP slopes for  $\text{MREC}_{N=3}$  and SISO are 3 and 1, respectively, which means that the AEP decreases much faster with  $\Gamma_s$  for  $\text{MREC}_{N=3}$  than for SISO.

Fig. 7 indicates that for  $\text{AS} < 4^\circ$ ,  $\text{MREC}_{N=2}$  generates almost the same SNR gain as  $\text{MREC}_{N=3:5}$  (which includes MRC). Furthermore, for  $\text{AS} < 10^\circ$ ,  $\text{MREC}_{N=3}$  generates almost the same SNR gain as  $\text{MREC}_{N=4:5}$ . Finally, for  $\text{AS} < 18^\circ$ ,  $\text{MREC}_{N=4}$  generates almost the same SNR gain as MRC. On the other hand, throughout the shown AS range,  $\text{MREC}_{N>1}$  greatly outperforms BF.

#### IV. PERFORMANCE AND COMPLEXITY COMPARISON OF BF, MRC, AND ADAPTIVE MREC FOR RANDOM AS

The above numerical results suggest that the MREC performance can be maximized by suitable selection of its order  $N$ . However, the order impacts the MREC numerical complexity, which translates into certain baseband-processing resource requirements [11], [12, ch. 5]. The numerical complexity of MRC and  $\text{MREC}_N$ , in terms of the number of complex multiplications and additions that are required per detected symbol

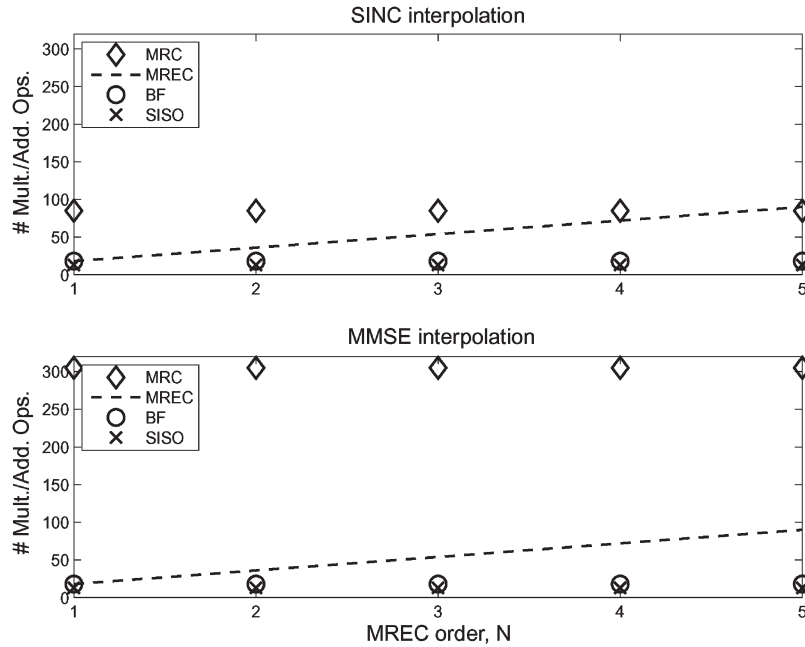


Fig. 8. Numerical complexity for SISO, BF,  $MREC_{N=1:L}$ , and MRC for exact combining,  $L = 5$ , and interpolator length  $T = 11$ . (Top) SINC interpolation. (Bottom) MMSE interpolation.

for interpolation, combining, and (only in MREC) for KLT, is reproduced in [12, Tab. 3.7, p. 132] and [13, Tab. II]. We have recently found that the MREC performance does not significantly degrade when the channel eigenstructure is updated by feeding received-signal samples into the deflation-based projection approximation subspace tracking (PASTd) algorithm [17]. Furthermore, PASTd-based eigenstructure tracking does not significantly increase the complexity of adaptive MREC because of PASTd's simplicity and because the eigenstructure changes very slowly (see [13, eq. (3)]).

Previous studies have indicated that exact and approximate implementations of MREC with SINC and MMSE PSAM have similar complexities due to the decorrelating effect of the KLT [12, Sec. 3.12], [13], [16], [17]. On the other hand, MRC can have much higher computational complexity for exact versus approximate combining and for MMSE versus SINC PSAM estimation.

Fig. 8 plots the numerical complexities computed from [13, Tab. II] for SISO, BF,  $MREC_{N=1:L}$ , and MRC, for  $L = 5$ , interpolator length  $T = 11$ , SINC and MMSE PSAM, and exact combining implementation. Note that for MMSE PSAM, MRC is much more complex than even full MREC because the channel gain vector that is required for MRC is estimated using matrix operations [12, eq. (3.113), p. 83], whereas the eigengains that are required for MREC are separately estimated as vectorial inner products [12, eq. (3.107), p. 82]. On the other hand, SINC PSAM inherently separates the estimation of the components of both the channel gain and eigengain vectors, so that the complexities of exact MRC and full-MREC are similar.

To minimize the MREC complexity and achieve near-MRC performance, we apply the simple and effective bias-variance tradeoff criterion (BVTC) [11], [12, Sec. 5.2.2], [13], [17] for exact-MREC order selection. For realistic performance

and complexity comparisons, a sufficient number (10 000) of independent lognormal AS samples for a typical urban scenario [13, Sec. II] have been generated with [13, eq. (2)]. The produced random AS sequence had an average of  $9.81^\circ$ , a standard deviation of  $13.4^\circ$ , and  $\Pr(1^\circ < AS < 20^\circ) \approx 0.83$ . For exact SISO, BF, MRC, and adaptive MREC with MMSE PSAM, Fig. 9 shows the means over the AS samples of the outage probabilities for QPSK—computed with (19), for  $P_{e,th} = 10^{-2}$  or, equivalently, for  $\gamma_{th} = 8.2$ —and of the computational complexities (computed from [13, Tab. II]). For reference, the lower subplot also displays a scaled version of the MREC order output by the BVTC, i.e.,  $10N$ . Note that, since the numerical complexities of SISO, BF, and MRC are AS- and  $\Gamma_s$ -independent, they do not require averaging. On the other hand, for MREC, the order output by the BVTC (and, thus, the numerical complexity) depends on AS and  $\Gamma_s$ . Fig. 9 indicates that the BVTC MREC order increases with increasing  $\Gamma_s$ , which improves the MREC performance but also increases complexity.

Fig. 9 shows that throughout the SNR range, adaptive MREC yields MRC-like performance, which can be much better than for BF due to the diversity gain and additional array gain. The OP performance level  $P_o = 10^{-1}$ , for instance, is achieved with SISO for  $\Gamma_s \approx 22$  dB and with BF for  $\Gamma_s \approx 16$  dB. Thus, BF produces an array gain of about 6 dB over SISO, which is about 1 dB lower than that achievable in ideal conditions, i.e.,  $10 \log_{10} L|_{L=5} \approx 7$  dB, for  $L = 5$  coherent and perfectly-known channel gains. MRC and BVTC-based adaptive MREC yield an extra 4-dB gain. At  $\Gamma_s = 12$  dB, the BVTC outputs an average order of  $N_{avg} \approx 2.86$  for MREC. Then, based on [13, Tab. II], we found that for MMSE PSAM, BVTC MREC is 2.86 and 3.96 times more complex than BF and SISO, respectively, but 5.92 times less complex than MRC.

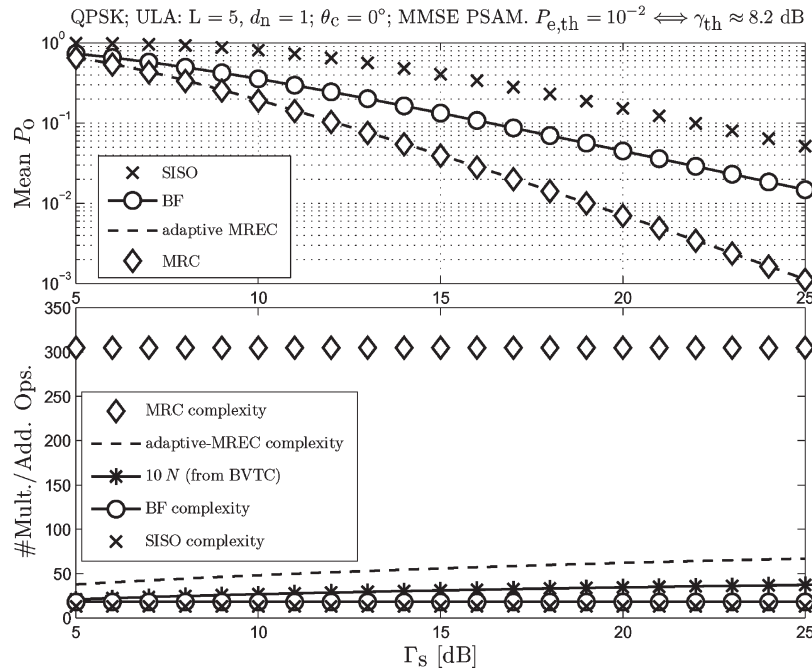


Fig. 9. (Top) OP for QPSK, averaged over 10 000 lognormal azimuth spread samples, for exact SISO, BF, MRC, and MREC adapted with the BVTC, for  $L = 5$ , and MMSE interpolation with  $T = 11$ . (Bottom) Corresponding numerical complexity.

For SINC PSAM and the same random AS sequence, other (not shown) numerical results have indicated that  $P_o = 10^{-1}$  is achieved with MRC and with BVTC-based adaptive MREC of average order  $N_{\text{avg}} \approx 3.02$  for  $\Gamma_s \approx 14$  dB, with BF for  $\Gamma_s \approx 18$  dB and with SISO for  $\Gamma_s \approx 24$  dB. Thus, the relative performance of these combining methods has not changed compared with the case of MMSE PSAM. However, while  $P_o = 10^{-1}$  is achieved for MMSE PSAM with adaptive MREC with  $N_{\text{avg}} \approx 2.86$  at  $\Gamma_s \approx 12$  dB, SINC PSAM requires  $N_{\text{avg}} \approx 3.02$  at  $\Gamma_s \approx 14$  dB, i.e., not only a 2-dB performance loss but also an increase of about 6% in complexity. SISO and BF experience the same performance loss but no complexity change for SINC PSAM versus MMSE PSAM. On the other hand, exact MRC experiences a 2-dB performance loss that is compensated by a 3.6-fold complexity reduction with SINC PSAM compared with MMSE PSAM.

Numerical results that are analogous to those from Fig. 9 have appeared for the AEP based on analysis and simulations in [12, Fig. 4.5, p. 149] and [13, Fig. 2]. Results that show the AEP versus time for temporally correlated samples of lognormal AS appear in [11, Fig. 5], [12, Fig. 4.6, p. 151], [13, Fig. 3], and [17, Figs. 4 and 5]. In [11] and [12, ch. 5], we demonstrated for fixed-point field-programmable-gate-array (FPGA)-based implementations that the lower average complexity of adaptive MREC versus MRC translates into reduced processing resource requirements and power consumption for the former. It has also been found that adaptive MREC could benefit from the AS independence among subscriber stations [11, Figs. 5–9], [12, Figs. 5.5–5.15, pp. 170–187]. Subscribers experiencing high AS can be allocated more base-station eigenprocessing modules [11, Sec. 2.5, p. 4], [12, p. 170] for better performance, which yields AS diversity.

## V. CONCLUSION

This paper completes earlier performance and numerical complexity studies of receive-side optimum (exact) MREC versus statistical BF and MRC. A novel closed-form expression has been derived for the pdf of the output SNR of MREC that seamlessly applies for p.k.c. or i.k.c. and an arbitrary fading correlation value, i.e., any combination of array interelement distance, mean angle of arrival, p.a.s. type, and AS value. This expression also applies to BF and MRC for smart antenna receivers, as well as to MRC and MREC for correlated “rake” receiver taps in CDMA systems. This pdf expression has been used to derive widely applicable closed-form expressions for the OP and the AEP of MREC, BF, and MRC. The advantages of MREC over BF and MRC have been analyzed in terms of the AF, deep-fade probability, diversity and array gains, OP, and numerical complexity. For realistic (Laplacian) base-station p.a.s. and lognormal AS, optimum channel fading estimation, and optimum combining implementation, adaptive MREC has been shown to achieve near-optimum average performance at a fraction of the MRC complexity. Thus, adaptive MREC has emerged as a practical alternative to the conventional—BF and MRC—approaches for smarter antennas as well as for more efficient CDMA receivers.

## APPENDIX

### SPECIAL-CASE CLOSED-FORM EXPRESSIONS FOR PERFORMANCE MEASURES FOR EXACT MREC

#### A. Case When All Eigenvalues Are Equal

In this case,  $\Gamma_i \triangleq \Gamma$ ,  $i = 1 : N$ , and the r.m.g.f. expression from (12) reduces to [3, eqs. (5.2–14), p. 319],

[4, eqs. (10)–(61), p. 310]

$$F_\gamma(s) = \frac{1}{(1+s\Gamma)^N} \quad (29)$$

whose inverse Laplace transform is

$$p(\gamma) = \frac{\gamma^{N-1} e^{-\gamma/\Gamma}}{(N-1)! \Gamma^N}. \quad (30)$$

Substituting this into the OP definition from (3) yields, for exact MREC, the following closed-form OP expression [3, eqs. (5.2–15), p. 319], [4, eqs. (10)–(64), p. 310]:

$$P_o = 1 - e^{\gamma_{th}/\Gamma} \sum_{n=0}^{N-1} \frac{1}{n!} \left( \frac{\gamma_{th}}{\Gamma} \right)^n. \quad (31)$$

Furthermore, with the notation  $\Upsilon \triangleq \Gamma g_{\text{PSK}}$ , the finite-limit integral exact-MREC AEP expression for M-PSK from (20) becomes

$$P_e = \frac{1}{\pi} \int_0^{\frac{M-1}{M}\pi} \left( 1 + \Upsilon \frac{1}{\sin^2 \phi} \right)^{-N} d\phi. \quad (32)$$

With the notations  $\xi \triangleq \sqrt{\Upsilon/\Upsilon+1}$ ,  $\alpha \triangleq \xi/\tan(\pi/M)$ , and  $\varphi \triangleq \tan^{-1} \alpha$ , the above can be written in closed form as [6, eqs. (5A.17–19), pp. 127–128]

$$P_e = \frac{M-1}{M} - \frac{\xi}{\pi} \sum_{n=0}^{N-1} \binom{2n}{n} \left( \frac{1-\xi^2}{4} \right)^n \times \left\{ \frac{\pi}{2} + \varphi + \sin \varphi \sum_{i=1}^n \frac{4^{(n-i)} [\cos \varphi]^{2(n-i)+1}}{\binom{2(n-i)}{n-i} [2(n-i)+1]} \right\} \quad (33)$$

where  $\binom{a}{b}$  represents the binomial coefficient, i.e.,  $\binom{a}{b} \triangleq a! / ((a-b)!b!)$ , and  $a! \triangleq a \cdot (a-1) \cdot (a-2) \cdots 3 \cdot 2 \cdot 1$ .

BPSK implies  $\varphi = 0$ , and therefore, (33) reduces to Proakis' expression [5, App. C, eq. (C-18), p. 955], i.e.,

$$P_e = \frac{1}{2} \left[ 1 - \xi \sum_{n=0}^{N-1} \binom{2n}{n} \left( \frac{1-\xi^2}{4} \right)^n \right] \quad (34)$$

which can also be written as [6, eq. (5A.4b), p. 125]

$$P_e = \left[ \frac{1}{2}(1-\xi) \right]^n \sum_{n=0}^{N-1} \binom{N-1+n}{n} \left[ \frac{1}{2}(1+\xi) \right]^n. \quad (35)$$

### B. Case When All Eigenvalues Are Distinct

In this case,  $N_d = N$  and  $r_k = 1, \forall k = 1 : N$ , so that (14) and (15) yield

$$F_\gamma(s) = \sum_{i=1}^N c_i \frac{1}{1+s\Gamma_i} \quad (36)$$

where

$$c_i = \prod_{j \neq i}^N \frac{\Gamma_j}{\Gamma_i - \Gamma_j}. \quad (37)$$

Then, the pdf of  $\gamma$ , i.e., the inverse Laplace transform of  $F_\gamma(s)$ , has the following simple closed-form expression:

$$p(\gamma) = \sum_{i=1}^N c_i \frac{1}{\Gamma_i} e^{-\gamma/\Gamma_i}. \quad (38)$$

For p.k.c., the above reduces to [4, eq. (10–60), p. 308]. From (3) and (38), the OP for  $M$ -PSK and exact MREC is

$$P_o = \sum_{i=1}^N c_i (1 - e^{-\gamma_{th}/\Gamma_i}). \quad (39)$$

Using (21) and (22), the AEP is obtainable as follows:

$$P_e = \frac{1}{2} \sum_{i=1}^N c_i \left( 1 - \sqrt{\frac{\Gamma_i g_{\text{PSK}}}{\Gamma_i g_{\text{PSK}} + 1}} \right). \quad (40)$$

For BPSK, this reduces to [19, eq. (16)]. For BPSK, p.k.c., and uncorrelated branches, (40) reduces to the ideal-MRC AEP formula proposed by Proakis [5, eq. (14.5–28), p. 847].

### REFERENCES

- [1] A. Paulraj, R. Nabar, and D. Gore, *Introduction to Space-Time Wireless Communications*. Cambridge, U.K.: Cambridge Univ. Press, 2005.
- [2] H. L. V. Trees, *Optimum Array Processing: Part IV of Detection, Estimation, and Modulation Theory*. New York: Wiley, 2002.
- [3] W. C. Jakes, Ed., *Microwave Mobile Communications*. New York: Wiley, 1974.
- [4] W. C. Y. Lee, *Mobile Communications Engineering*. Englewood Cliffs, NJ: McGraw-Hill, 1982.
- [5] J. G. Proakis, *Digital Communications*, 4th ed. New York: McGraw-Hill, 2001.
- [6] M. K. Simon and M.-S. Alouini, *Digital Communication Over Fading Channels. A Unified Approach to Performance Analysis*. Baltimore, MD: Wiley, 2000.
- [7] S. Choi, J. Choi, H.-J. Im, and B. Choi, "A novel adaptive beamforming algorithm for antenna array CDMA systems with strong interferers," *IEEE Trans. Veh. Technol.*, vol. 51, no. 5, pp. 808–816, Sep. 2002.
- [8] R. Vaughan and J. B. Andersen, *Channels, Propagation and Antennas for Mobile Communications*. London, U.K.: Inst. Elect. Eng., 2003.
- [9] D. G. Brennan, "Linear diversity combining techniques," *Proc. IEEE*, vol. 91, no. 2, pp. 331–356, Feb. 2003.
- [10] J. Choi and S. Choi, "Diversity gain for CDMA systems equipped with antenna arrays," *IEEE Trans. Veh. Technol.*, vol. 52, no. 3, pp. 720–725, May 2003.
- [11] C. Siriteanu, S. D. Blostein, and J. Millar, "FPGA-based communications receivers for smart antenna array embedded systems," *EURASIP J. Embedded Syst.—Special Issue on Field-Programmable Gate Arrays in Embedded Systems*, vol. 2006, pp. 1–13, 2006. Article ID 81 309.
- [12] C. Siriteanu, "Maximal-ratio eigen-combining for smarter antenna array wireless communication receivers," Ph.D. dissertation, Queen's Univ., Kingston, ON, Canada, 2006.
- [13] C. Siriteanu and S. D. Blostein, "Maximal-ratio eigen-combining for smarter antenna arrays," *IEEE Trans. Wireless Commun.*, vol. 6, no. 3, pp. 917–925, Mar. 2007.
- [14] C. Sun, J. Cheng, and T. Ohira, Eds., *Handbook on Advancements in Smart Antenna Technologies for Wireless Networks. Chapter 'Eigencombining: A Unified Approach to Antenna Array Signal Processing'* by C. Siriteanu and S. D. Blostein. New York: Idea Group, 2009.
- [15] C. Brunner, W. Utschick, and J. A. Nossek, "Exploiting the short-term and long-term channel properties in space and time: Eigenbeamforming

concepts for the BS in WCDMA," *Eur. Trans. Telecommun.—Special Issue on Smart Antennas*, vol. 12, no. 5, pp. 365–378, Sep./Oct. 2001.

- [16] C. Siriteanu and S. D. Blostein, "Diversity combining and eigencombining performance and complexity comparison for estimated channels," in *Proc. 24th Biennial Symp. Commun.*, Kingston, Canada, 2008, pp. 128–133.
- [17] C. Siriteanu, G. Xin, and S. D. Blostein, "Performance and complexity comparison of MRC and PASTd-based statistical beamforming and eigencombining," in *Proc. 14th APCC*, Tokyo, Japan, 2008. Session 16-PM1-A.
- [18] J. Jelitto and G. Fettweis, "Reduced dimension space-time processing for multi-antenna wireless systems," *IEEE Wireless Commun.*, vol. 9, no. 6, pp. 18–25, Dec. 2002.
- [19] F. A. Dietrich and W. Utschick, "Maximum ratio combining of correlated Rayleigh fading channels with imperfectly known channel," *IEEE Commun. Lett.*, vol. 7, no. 9, pp. 419–421, Sep. 2003.
- [20] F. Patenaude, J. Lodge, and J.-Y. Chouinard, "Eigen analysis of wide-band fading channel impulse responses," *IEEE Trans. Veh. Technol.*, vol. 48, no. 2, pp. 593–606, Mar. 1999.
- [21] V. A. Aalo, "Performance of maximal-ratio diversity systems in a correlated Nakagami-fading environment," *IEEE Trans. Commun.*, vol. 43, no. 8, pp. 2360–2369, Aug. 1995.
- [22] P. Lombardo, G. Fedele, and M. M. Rai, "MRC performance for binary signals in Nakagami fading with general branch correlation," *IEEE Trans. Commun.*, vol. 47, no. 1, pp. 44–52, Jan. 1999.
- [23] D. Tse and P. Viswanath, *Fundamentals of Wireless Communication*. Cambridge, U.K.: Cambridge Univ. Press, 2005.
- [24] C. Siriteanu and S. D. Blostein, "Maximal-ratio eigencombining: A performance analysis," *Can. J. Elect. Comput. Eng.*, vol. 29, no. 1/2, pp. 15–22, Jan.–Apr. 2004.
- [25] I. S. Gradshteyn and I. M. Ryzhik, *Table of Integrals, Series, and Products*, 4th ed. New York: Academic, 1965.
- [26] E. G. Larsson and P. Stoica, *Space-Time Block Coding for Wireless Communications*. Cambridge, U.K.: Cambridge Univ. Press, 2003.
- [27] M. Abramowitz and I. A. Stegun, Eds., *Handbook of Mathematical Functions With Formulas, Graphs and Mathematical Tables*. New York: Dover, 1995.



**Steven D. Blostein** (SM'83–M'88–SM'96) received the B.S. degree in electrical engineering from Cornell University, Ithaca, NY, in 1983 and the M.S. and Ph.D. degrees in electrical and computer engineering from the University of Illinois, Urbana-Champaign, in 1985 and 1988, respectively.

Since 1988, he has been with the faculty of Queen's University, Kingston, ON, Canada, where he currently holds the position of Professor and is the Head of the Department of Electrical and Computer Engineering. From 1999 to 2003, he was the Leader of the Multi-Rate Wireless Data Access Major Project sponsored by the Canadian Institute for Telecommunications Research. He has also been a consultant to government and industry in the areas of image compression, target tracking, radar imaging, and wireless communications. In 1994 and 1995, he was with the Lockheed Martin Electronic Systems, Montreal, QC, Canada, and in 2006, he was with the Communications Research Centre, Ottawa, ON. He has been a Member of the Samsung 4G Wireless Forum, as well as an invited Distinguished Speaker with Ryerson University, Toronto, ON, and Samsung Advanced Institute of Technology. His current interests include the application of signal processing to wireless communications systems, including smart antennas, multiple-input-multiple-output (MIMO) systems, and space-time-frequency processing for MIMO-orthogonal frequency division multiplexing systems.

Dr. Blostein is a Registered Professional Engineer in Ontario. He served as the Chair of the IEEE Kingston Section in 1994, the Chair of the Biennial Symposium on Communications in 2000, 2006, and 2008, as an Associate Editor for the IEEE TRANSACTIONS ON IMAGE PROCESSING during 1996–2000, and as Publications Chair for the IEEE International Conference on Acoustics, Speech, and Signal Processing in 2004. He is currently serving as an Editor for the IEEE TRANSACTIONS ON WIRELESS COMMUNICATIONS.



**Constantin Siriteanu** was born in Sibiu, Romania, in 1972. He received the B.S. and M.S. degrees in electrical engineering from the "Gheorghe Asachi" Technical University, Iasi, Romania, in 1995 and 1996, respectively, and the Ph.D. degree in electrical engineering from Queen's University, Kingston, ON, Canada, in 2006.

Between 1995 and 1997, he was a part-time Engineer with the Research Institute for Automation, Iasi, where he worked on data transmission over power lines. Between 1996 and 1998, he was a Research

Assistant with the Department of Automatic Control and Computer Science, "Gheorghe Asachi" Technical University, where he worked on digital control systems. Between September 2006 and February 2008, he was a Postdoctoral Researcher with Hanyang University, Seoul, Korea, where he also taught a graduate course on multiple-input-multiple-output systems. Subsequently, he was a Visiting Assistant Professor with Kyungpook National University, Daegu, Korea, for one term. Since June 2008, he has been a "Brain Korea" Assistant Professor with Seoul National University. His research interests include reduced-complexity signal processing for multibranch wireless communications transceivers.